GL01323

IR

An Advanced Airborne Infrared Method for Evaluating Geothermal Resources

N. KERR DEL GRANDE

Lawrence Livermore Laboratory, University of California, Livermore, California 94550, USA

ABSTRACT

A new geophysical assessment method, which (1) identifies most geothermal resources with few ground measurements; (2) quantifies *weak heat flows*, five or more times the global average; and (3) pinpoints areas for deep exploratory drilling is described. This capability does not currently exist. Aerial thermal surveys have duplicated results of shallow thermal gradient surveys for measuring heat flows greater than 3 W/m^2, enhancing the surface temperature more than 0.5 K above the ambient value. The Geothermal Energy Multiband (GEM) system, which would have 10 times better sensitivity, is described. Such a system is needed to reduce the time and cost of detailed thermal surveys (typically 1-1/2 yr and $2 to $3 million) prior to deep exploratory drilling of promising geothermal sites. Near-surface heat-flow measurements require 125 000 man-hours per 100 km^2. Aerial thermal surveys require only 5 man-hours to scan 100 km^2 four separate times and cost less than $100 000.

The GEM system would resolve 0.05 to 0.5 K temperature enhancements for areas more than 1 km^2 by ratioing narrow infrared (ir) bands at 2.2, 3.5, 3.9, 4.8 and 13.2 μm. These *signal ratios* have major advantages, namely (1) they are insensitive to the surface emissivity for natural terrains; (2) they vary as a high power of the absolute surface temperature (typically $50/\lambda_1$ to $50/\lambda_2$ near 288 K for ir wavelengths at λ_1 and λ_2 μm); and (3) they avoid the 6- to 13-μm region (subject to interpretive uncertainties from 0.5 to 5 K for surfaces composed of silicates, carbonates, and sulfates). Four predawn surveys taken under varied climatic conditions are needed to provide redundant data for distinguishing geothermal effects from climatic thermal noise. Differences in the spatial-thermal relationships caused by variations in the wind velocity, soil moisture, humidity, topography, or hydrology would be identified and removed by data processing.

INTRODUCTION

Geothermal energy is one of the more promising of the unconventional energy sources now being considered for the future. The U.S. goal is to stimulate commercial production from geothermal resources of 20 GW by 1985 and 200 GW by 2020 (Ray, 1973). To achieve these goals it will be necessary to develop more effective, efficient, and economical geophysical exploration methods.

The potentially valuable geothermal resource base of the country occupies some 390 000 km^2 (96 million acres) in the western third of the conterminous U.S. (Godwin et al., 1971). These lands must be evaluated as the exact location, size, and potential of the geothermal fields are almost unknown (Anderson and Axtell, 1972). Before an electric power company will even consider constructing a generating plant, it insists on proof of a 200 to 400 MW potential. This means drilling 10 to 12 wells, which normally takes 2 yr and costs from $3 to $6 million (Loehwing, 1974). This paper describes a new geophysical assessment method, which (1) identifies most geothermal resources with few ground measurements; (2) quantifies *weak heat flows*, five or more times the global average; and (3) pinpoints areas for deep exploratory drilling. The concept is called the Geothermal Energy Multiband (GEM) system. This capability does not currently exist. Once developed, the method should be able to provide detailed aerial thermal surveys at a small fraction of the cost (in both time and money) of existing methods. Detailed thermal surveys for large geothermal fields require typically 1-1/2 yr and cost $2 to $3 million prior to deep exploratory drilling. Geothermal heat-flux measurements require 125 000 man-hours per 100 km^2 using conventional methods (Dawson and Dickinson, 1970). Aerial methods should require only 5 man-hours to scan 100 km^2 four separate times and cost less than $100 000. The availability of an advanced airborne infrared method for geothermal prospecting would stimulate the large-scale evaluation of geothermal resources by small as well as large companies.

EXISTING AERIAL INFRARED METHODS

Under good conditions, current aerial infrared methods can identify regions on the Earth's surface that are as little as 0.5 K warmer than the ambient temperature. Geothermal fluxes of about 50 times the global average for nongeothermal areas manifest surface thermal anomalies of this magnitude. (The global average heat flow is about 1.5 heat-flow units, 0.06 W/m^2.) New geothermal areas (in Italy, Hodder et al., 1973; and in New Zealand, Dickinson, 1973) were successfully located with aerial infrared surveys. The results of these surveys agreed with the data obtained from shallow thermal-gradient surveys for heat flows greater than 3 W/m^2. Conditions were such that other aerial surveys have only been able to detect the surface expression of intrinsic heat flows ranging from 100 to 500 times the global average

(White and Miller, 1969; Palmason et al., 1970; Hochstein and Dickinson, 1970). For aerial surveys to be most useful they should be able to detect surface-temperature anomalies as small as 0.05 to 0.5 K extending over an area of a few tens to a few hundreds of square kilometers. Detecting such areas requires a factor-of-ten improvement in existing temperature sensitivity, and a methodology for removing from the data the temperature effects not related to geothermal activity—effects caused by meteorology, hydrology, topography, and terrain conditions. Recent work, mostly at the Lawrence Livermore Laboratory (LLL), has shown that it may be possible to achieve both of these objectives.

GEOTHERMAL ENERGY MULTIBAND CONCEPT

Existing aerial infrared scanning systems measure radiation emitted by the terrain in one or at most two infrared bands near the peak of the spectrum radiated by the terrain. These systems have NET (noise-equivalent-temperature) responses that allow them to discriminate temperature differences of 0.5 K over flat, homogeneous terrain. However, the measured signals must be calibrated against an ideal (blackbody) source that radiates with 100% efficiency. The Earth's surface is a less efficient radiator. The interpretability of temperature differences is affected by the emissivity variations that characterize different natural terrains. Temperature rises from 0.5 to 5 K are usually obscured by these emissivity effects.

We have conceived a multiband system that makes use of the radiation emitted in seldom-used atmospheric pass bands at 2.2, 3.5, 3.9, 4.8, and 13.2 μm. By using ratios of measurements made in these bands, we can realize several major advantages:

1. Surface emissivity effects for natural terrains are small and can be eliminated using analytical techniques.
2. The ratios vary as a high power of the absolute surface temperature, with the result that smaller temperature differences can be detected. Our calculations, given in the appendix, show that for typical predawn temperatures the radiant emittance (power per unit area) of a surface varies as the $50/\lambda$ power of the absolute temperature, where λ is the detected wavelength in micrometers. Thus, for the 3.5-μm band the emittance varies as the 14th power of the temperature.
3. One can avoid those ir wavelength regions in which the interpretation is subject to uncertainties from 0.5 to 5 K. These large uncertainties are associated with wavelengths at which the terrain radiates as a specular source; that is, the surface emissivity varies greatly with wavelength. This occurs for minerals containing certain anions, such as silicate, sulfate, and carbonate (Lyon, 1964; Vincent, 1973).

Figure 1 indicates the wavelengths at which the Earth's radiation (dashed curves) has the same slope as that of an ideal blackbody source (solid curves). The shaded bands are the atmospheric windows that avoid wavelengths at which the terrain behaves as a specular source. These windows are the wavelengths the GEM system uses.

Signal ratios of bands at these wavelengths can be used to resolve 0.05 to 0.5 K temperature rises over areas larger than 1 km^2. The bands must be coregistered; the instrumental scanning speeds must be adjusted to obtain good counting statistics; and the filters must be cooled to liquid-nitrogen temperatures for distinguishing temperature effects as low as 0.05 K, with large area sensors and an optical system that resolves 50 m at an altitude of 3 km (Larsen, 1971; private commun., 1974).

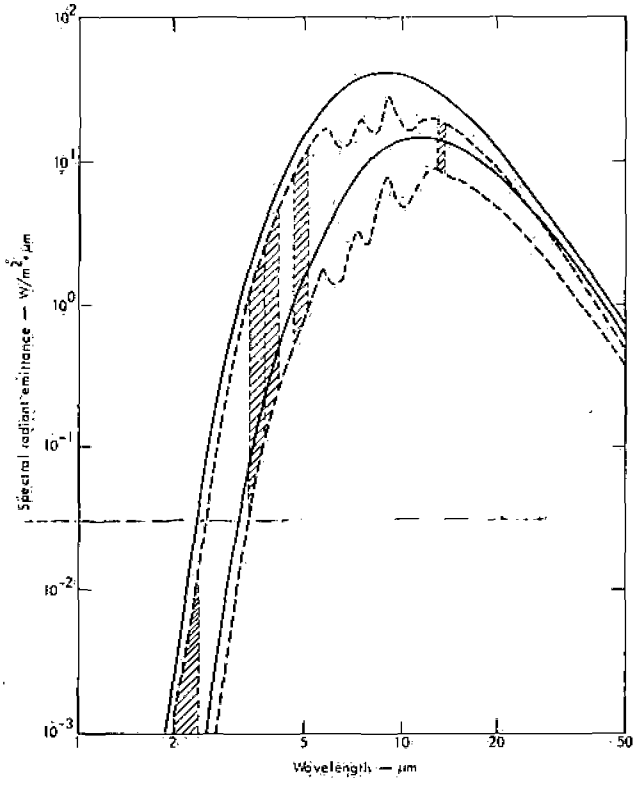

Figure 1. Infrared emission from the Earth's surface. The solid curves represent ideal blackbody sources at 318 K (top curve) and 258 K (bottom curve). The corresponding dashed curves have an emissivity less than one, like the natural terrain. The shaded areas are the atmospheric windows that occur at wavelengths where the Earth's radiation has the same slope as an ideal blackbody source. These are the GEM wavelengths.

REMOVING NONGEOTHERMAL EFFECTS

To enhance the detectability of geothermal anomalies several procedures are required: (1) aerial surveys should be taken when the environmental conditions do not obscure geothermal anomalies; (2) the temperature data must be corrected for minor emissivity effects, the intervening atmospheric path, and reflected sky radiation; and (3) thermal anomalies identifiable with meteorological, hydrological, topographical, or soil thermal conditions must be removed from the data. We have developed a methodology that will perform these tasks.

For optimum measuring conditions the aerial surveys should be taken before dawn, when the terrain has reached a diurnal equilibrium temperature and winds are less than 1.3 m/sec (3 mph). This enhances the thermal contrast originating from geothermal effects.

To distinguish between the anomalies associated with surface emissivity variations and those associated with geothermal activity, we use an emmissivity-dependent function obtained from the multiband ir data. To correct for the intervening atmospheric path and reflected sky radiation, we determine the air temperature at the surface and sensor

altitudes, the relative humidity, and the cloud-cover conditions (Tien, 1974). Surface radiometric measurements and aerial thermal surveys at different altitudes give empirical methods for making atmospheric corrections (Shaw and Irbe, 1972; Saunders, 1970; Weiss, 1971).

Thermal anomalies associated with meteorological, hydrological, topographical, and soil-thermal conditions can be calculated. To do this we simulate the surface temperatures (assuming no geothermal activity) using a digital surface-climate model that accounts for the effects of some 15 measurable environmental parameters (Outcalt, 1972a, b, and c). In geothermal areas, temperature anomalies of 0.05 to 0.5 K above ambient would appear as a residual difference between the measured-and-corrected surface temperatures and the surface temperatures calculated using the surface-climate model (Outcalt, 1972a).

Geothermal anomalies, unlike thermal anomalies associated with the climate, would change very little from season to season and would be relatively independent of the topography. Aerial surveys taken under varied climatic conditions four times during the year would provide redundant data for distinguishing nongeothermal effects. Differences in the spatial-thermal relationships caused by variations in the wind velocity, soil moisture, humidity, topography, or hydrology would be identifiable from the imagery and calculable using the climatological model.

Signal processing techniques offer yet another way for sorting out the complexities of thermal infrared imagery. Analytical techniques have been developed that test the degree to which any two wavelength measurements obey the Planckian relationships for blackbody (or graybody) radiation. Statistical tests are able to sort out subtle emissivity effects related to the thermal diffusivity of the soil, the surface-moisture content, and the surface-thermal conditions.

The data can be Fourier-analyzed for determining high- and low-frequency spatial-thermal effects. This makes it possible to distinguish between thermal effects encompassing a relatively large area (the geothermal resource area) and thermal effects confined to small climatological regimes. Many geothermal anomalies, though small in thermal magnitude, would be characterized by an above-average temperature extending over a large area (a few tens to a few hundreds of square kilometers). Climatological, hydrological, and topographical anomalies are distinguishable by their size and shape, which differ significantly from the features that characterize geothermal fields.

The amount of data collected with aerial survey methods is enormous. It is not expected that each and every anomaly will be identifiable with a likely source of heat. Rather, the major data trends will be identifiable with the major sources of thermal variations. Cluster algorithms are used to identify distinct thermal regimes from the raw data. Techniques are being developed to remove data not belonging to any distinct thermal regime.

We are developing data processing methods that display two- and three-dimensional plots of temperature versus surface position, average temperatures for specified areas, temperatures that have been corrected for emissivity, the intervening atmospheric path and reflected sky radiation, and temperatures based on the simulated climatological conditions. Statistical methods will be used to deduce whether the differences between the corrected temperature data for a geothermal area and the simulated temperature data are significant.

Surface-contact temperature measurements play an important role in the development of quantitative aerial thermal surveys. They can be used to give an independent test of the surface temperature that can be compared with the aerial survey measurements and the simulated surface temperatures. A meteorological tower is instrumented to measure environmental conditions (for example, the wind velocity, relative humidity, soil moisture, and solar insolation). Radiometric surface measurements provide supplementary data on the surface emissivity and atmospheric corrections.

PRELIMINARY TEST WITH DUAL-BAND SYSTEM

We have made preliminary tests of our data-analysis method using already-existing dual-band ir data recorded in narrow ir bands centered at about 5 and 10 μm. These data were taken by the National Oceanic and Atmospheric Administration (NOAA) over vegetated terrain in upstate New York (Peck, Bissell, and Farnsworth, 1972). We found that the ratios of the signals recorded at the two bands had the desired properties: they were insensitive to surface emissivity variations; they varied nearly as the fifth power of the surface temperature, as predicted by our power-law-thermal model; and they could be used to isolate emissivity-related effects.

Working with the Development and Resources Transportation Company (Silver Spring, Maryland) we were able to characterize the observed surface-temperature variations and separate out the purely emissivity-related features of the terrain (LeSchack et al., 1975; LeSchack and Del Grande, 1975). With the 5-μm signal, the emissivity ratio, and the soil moisture of 34 ground samples as input parameters, we used a cluster analysis method that showed that the raw-radiant-emittance data fell into two distinct terrain groups. An independent test showed that this dichotomy was based on the condition of the surface vegetation; one group was characterized by dry, dying vegetation and the other by viable, green vegetation. Using corrections based on this analysis, we adjusted the airborne radiant-temperature measurements at 10 μm for surface-emissivity variations, the intervening atmospheric path, and the reflected sky radiation. We then compared the corrected surface-temperature data with the calculated values obtained using the surface-climate model. The calculated mean surface temperatures, 291.87 K for the dry vegetation 291.61 K for the green vegetation, differed by only 0.01 and 0.15 K respectively from the measured mean surface temperatures.

The natural temperatures at various locations on the test terrain at the time the NOAA data were taken varied from the mean temperature by as much as 2 K. However, we were able to discern that the mean temperature for the part of the terrain that lay at an altitude of 370 m was 0.2 K colder than the 290-m part. (This difference mainly results from the normal temperature drop with increasing altitude.) This topographical effect was distinguishable as a large-area 0.2-K temperature difference that was separable from temperature variations as large as 2 K characterizing small-area thermal regimes. The redundancy of data available from the aerial survey is sufficient to prove the effect as statistically significant. This is shown in Figure 2.

RECOMMENDATIONS FOR FUTURE STUDIES

A cooperative venture is now getting underway between ENSCO, Inc. (Springfield, Virginia), the Environmental

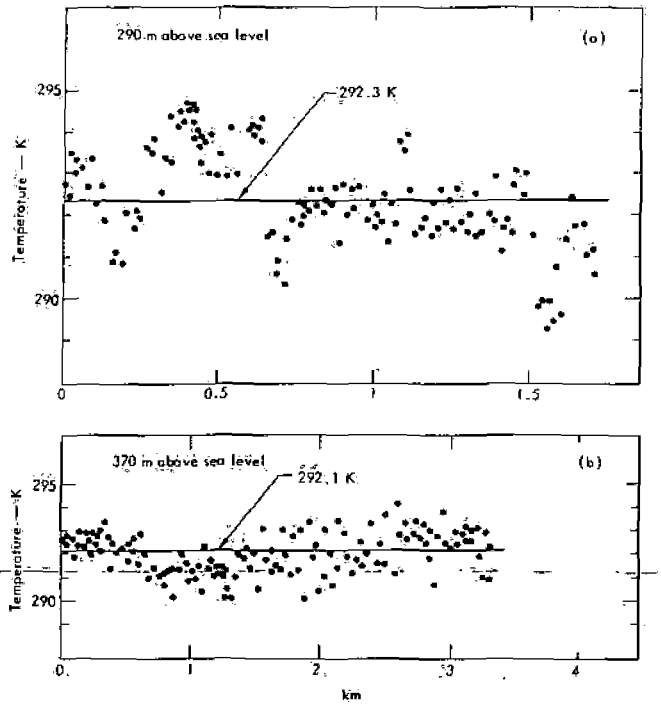

Figure 2. Temperature measurements from ratios of dual-band infrared surveys at 5 and 10 μm over vegetated terrain. The data for small areas of about 300 m² vary from the mean as much as 2 K at 15:27 solar time. By smoothing the data, the average temperatures for large areas of 70 000 (curve a) and 160 000 (curve b) m² were found to differ by 0.2 K. This difference mainly resulted from the normal temperature drop with increasing altitude.

Research Institute of Michigan (Ann Arbor), and LLL to test the feasibility of multiband detection for geothermal resource investigations. The existing multispectral scanner at ERIM will be modified to test the GEM concept. The methodology for quantitative aerial-surface temperature measurements will be evaluated over several nongeothermal areas in Michigan. Selected test areas will be measured by aerial- and surface-radiometric methods. The results will be compared with temperatures calculated using the surface-climate simulator model (Outcalt, 1972a) and with contact-temperature data taken at the surface and at shallow depths. If the results are as encouraging as those of the analysis of the New York NOAA data (LeSchack et al., 1975; LeSchack and Del Grande, 1975), we hope to be able to proceed with a full-scale effort to develop our aerial reconnaissance method as a routine geothermal prospecting technique.

SUMMARY AND CONCLUSIONS

We are developing a promising new aerial-reconnaissance method for identifying and evaluating potentially valuable geothermal resource areas. The method is based on a power-law-thermal model that describes the dependence on wavelength and temperature of the detectable radiation emitted by the terrain. Based on our calculations, we have designed a GEM (geothermal energy multiband) detection system. The GEM system uses signal ratios to attain a factor-of-ten improvement in instrumental temperature sensitivity. We are developing a methodology that will specify the environmental conditions for effective surveys and correct for nongeothermal effects. Preliminary tests of the methodology have successfully demonstrated the power-law-thermal model, the signal-ratio method and the climatological model used to simulate surface-temperature variations caused by nongeothermal effects. The differences between the mean temperatures measured over a nongeothermal area and those simulated using the climatological model were only 0.01 K for dry vegetation and 0.15 K for green vegetation. The development of our aerial reconnaissance method as a routine geothermal prospecting technique would make practical the large-scale evaluation of prospectively valuable geothermal resource lands estimated to encompass nearly 400 000 km² throughout the western third of the conterminous U.S.

ACKNOWLEDGMENTS

The author is grateful for the continued support and assistance of Drs. Jack N. Shearer and Paul Ebert of LLL. Further appreciation is extended to Professor Gunnar Bodvarsson (Oregon State University, Corvallis) and Newberry Professor Emeritus Paul Kerr (formerly of Columbia University) for valuable advice and the encouragement to carry out this work. The author thanks Dr. Donald Wiesnet (National Oceanic and Atmospheric Administration) for making the dualband infrared imagery available, Richard Neifert of LLL for his help in analyzing the film imagery, and Leonard LeSchack (Development and Resources Transportation Company, Silver Spring, Maryland) for many valuable discussions pertaining to the interpretation of infrared survey data for soil moisture studies and geophysical investigations. She also acknowledges the helpful suggestions by Dr. David Dickinson (Department of Scientific and Industrial Research, Wellington, New Zealand) and Dr. Robert M. Moxham (United States Geological Survey, Reston, Va.) pertaining to the interpretation of infrared imagery for geothermal studies. In addition, she thanks Leo M. Larsen (Environmental Research Institute of Michigan, Ann Arbor) for checking her calculations and evaluating the radiometric capabilities of infrared detectors utilized in line scanners. Finally, she extends her appreciation to Drs. Frank J. Cook and Richard Sebastian (ENSCO, Inc., Springfield, Virginia) for fruitful discussions related to signal processing techniques for data reduction as well as for their continued support and encouragement of this work.

This work was performed under the auspices of the U.S. Energy Research and Development Administration.

APPENDIX

The Power-Law Thermal Model

The special radiant emittance, W_λ, measured in units of (W/m²) per unit wavelength is what is detected by the airborne ir scanning system. Planck's equation expresses W_λ as follows:

$$W_\lambda = \epsilon_\lambda C_1 \lambda^{-5} [\exp(C_2/\lambda T) - 1]^{-1}, \quad (1)$$

where ϵ_λ = surface emissivity at a given wavelength; $C_1 = 3.7414 \times 10^8$ (W/m²)·μm⁴; $C_2 = 1.4388 \times 10^4$ μm·K;

λ = wavelength in μm; and T = surface temperature in K. Since the scanner senses not the entire range of emitted energy but only that energy contained in the wavelength band for which the system is designed, Eq. (1) should be expressed as

$$W = \int_{\lambda_1}^{\lambda_2} \epsilon_\lambda C_1 [\exp(C_2/\lambda T) - 1]^{-1} \lambda^{-5} d\lambda. \quad (2)$$

To simplify the mathematics we will make the following substitution:

$$y = C_2/\lambda T, \quad (3)$$

and it therefore follows that $\lambda = C_2/Ty$. By differentiating,

$$\lambda^{-5} d\lambda = -C_2^{-4} T^4 y^3 dy. \quad (4)$$

Equation (2) can now be rewritten

$$W = \int_{y_1}^{y_2} \frac{\epsilon_\lambda C_1}{\exp(y) - 1} (-C_2^{-4} T^4 y^3) dy^* \quad (5)$$

or

$$W = -\epsilon_\lambda C_1 C_2^{-4} T^4 \int_{y_1}^{y_2} \left[\frac{y^3}{\exp(y) - 1}\right] dy.^\dagger \quad (6)$$

Multiplying the numerator and denominator of the bracketed term by $\exp(-y)$ we have

$$\frac{y^3 \exp(-y)}{1 - \exp(-y)}$$

and

$$W = \epsilon_\lambda C_1 C_2^{-4} T^4 \int_{y_1}^{y_2} \left[\frac{y^3 \exp(-y)}{1 - \exp(-y)}\right] dy. \quad (7)$$

The term $\dfrac{\exp(-y)}{1 - \exp(-y)}$ can be expanded in a binomial series as

$$\exp^{-y} \sum_{m=0}^{\infty} \exp(-my) = \exp(-y)[\exp(-0) + \exp(-y) + \exp(-2y) + \ldots + \exp(-my)]$$

or $\{\exp(-y) + \exp(-2y) + \exp(-3y) + \ldots + \exp[-(m+1)y]\}$,

which can be expressed as

$$\sum_{m=1}^{\infty} \exp(-my).$$

Equation 7 can now be rewritten using the above expansion and eliminating the negative sign by reversing the limits of integration as follows:

$$W = \epsilon_\lambda C_1 C_2^{-4} T^4 \int_{y_2}^{y_1} y^3 \left[\sum_{m=1}^{\infty} \exp(-my)\right] dy. \quad (8)$$

Integrating Eq. (8) by parts, using the form

$$\int y^3 \exp(-my)\, dy = \frac{y^3 \exp(-my)}{-m} - \frac{3}{-m} \int y^2 \exp(-my)\, dy.$$

From Standard Mathematical Tables (1962), we obtain

$$W = \epsilon_\lambda C_1 C_2^{-4} T^4 \left[\sum_{m=1}^{\infty} \exp(-my_2)\left(\frac{y_2^3}{m} + \frac{3y_2^2}{m^2} + \frac{6y_2}{m^3} + \frac{6}{m^4}\right) - \sum_{m=1}^{\infty} \exp(-my_1)\left(\frac{y_1^3}{m} + \frac{3y_1^2}{m^2} + \frac{6y_1}{m^3} + \frac{6}{m^4}\right)\right]. \quad (9)$$

Equation (9) is a complete expansion of Planck's equation. However, it is unwieldy to evaluate.

Accordingly, we have derived an approximation of Eq. (9) that considerably simplifies the mathematics. It follows from Eq. (1), that is,

$$W_\lambda = \epsilon_\lambda C_1 \lambda^{-5} [\exp(C_2/\lambda T) - 1]^{-1}.$$

Differentiating Eq. (1) with respect to T and holding λ constant, we obtain

$$dW_\lambda = \epsilon_\lambda C_1 \lambda^{-5} \frac{(C_2/\lambda T^2) \exp(C_2/\lambda T)}{[\exp(C_2/\lambda T) - 1]^2} dT. \quad (10)$$

Dividing Eq. (10) by W_λ we obtain

$$\frac{dW_\lambda}{W_\lambda} = \frac{(C_2/\lambda T^2) \exp(C_2/\lambda T)}{[\exp(C_2/\lambda T) - 1]} dT, \quad (11)$$

or

$$\frac{dW_\lambda}{W_\lambda} = (C_2/\lambda T)\left[\frac{\exp(C_2/\lambda T)}{\exp(C_2/\lambda T) - 1}\right] \frac{dT}{T}. \quad (12)$$

The bracketed term, by multiplying and dividing by $\exp(-C_2/\lambda T)$, can be rewritten $\left[\dfrac{1}{1 - \exp(-C_2/\lambda T)}\right]$, which is of the form $\dfrac{1}{1-x}$, where $x = \exp(-C_2/\lambda T)$. It therefore can be expressed as a binomial expansion of the form

$$\frac{1}{1-x} = 1 + x + x^2 + \ldots + x^m = \sum_{m=0}^{\infty} x^m$$

* For integrations over small wavelength intervals, ϵ_λ is considered constant; λ applies to the mean wavelength.

† Substituting the Stefan-Boltzmann constant, σ, for $(\pi^4/15) C_1 C_2^{-4}$ and integrating from zero to infinity, we obtain the Stefan-Boltzmann Law: $W = \epsilon_\lambda \sigma T^4$ for the total hemispherical emittance.

as long as $\exp(-C_2/\lambda T) \ll 1$. This will be the case since $(C_2/\lambda T)$ is positive. With the nominal temperature of 15°C or 288 K and for data recorded in wavelengths less than 15 μm, the bracketed term is approximately equal to unity; this is because the second and higher order terms of the expansion are much less than 1.

Accordingly, Eq. (12) can be expressed as

$$\frac{dW_\lambda}{W_\lambda} \cong \frac{C_2}{\lambda T}\frac{dT}{T} \cong \frac{C_2}{\lambda T_o}\left[1 - \frac{\Delta T}{T_o} + \left(\frac{\Delta T}{T_o}\right)^2 - \cdots + \left(\frac{-\Delta T}{T_o}\right)^m\right]\frac{dT}{T}.^* \quad (13)$$

Since by definition $\frac{dW_\lambda}{W_\lambda} \equiv d\ln W_\lambda$, and $\frac{dT}{T} \equiv d\ln T$ for small variations in T, Eq. (13) can be approximated by

$$d\ln W_\lambda \cong \frac{C_2}{\lambda T_o} d\ln T \cong d\ln T^{C_2/\lambda T_o}. \quad (14)$$

Integrating Eq. (14) we obtain

$$\ln W_\lambda \cong \ln T^{C_2/\lambda T_o} + C_3,$$

where C_3 is a constant of integration that includes ϵ_λ and

$$W_\lambda \propto \epsilon_\lambda T^{C_2/\lambda T_o}. \quad (15)$$

For $C_2 = 14\,388$ μm·K and a nominal value of $T_o = 288$ K, $C_2/T_o = 49.96$, Eq. (15) can be closely approximated by

$$W_\lambda \propto \epsilon_\lambda T^{50/\lambda}. \quad (16)$$

We have computed the difference for a 1 K change of W_λ from $T = 288$ K to $T = 289$ K by evaluating Eq. (9), the complete expansion of Planck's equation, and Eq. (15). Comparing the results, we found that for the wavelengths of most interest to us (that is, the GEM wavelengths from 3 to 13 μm) the signal response calculated from Eq. (15) introduces an error of no more than 0.04%.

We have derived a convenient expression for calculating the temperature sensitivity of aerial infrared scanning systems. At a typical predawn temperature of 288 K, the detectable radiation is proportional to $\epsilon_\lambda T^{50/\lambda}$. Filters are used to define narrow bands. A few bands avoid both atmospheric absorption regions, and wavelengths associated with anion groups in common minerals where the terrain behaves as a specular source. They are centered at 2.2, 3.5, 3.9, 4.8 and 13.2 μm. These are the GEM wavelengths. At these wavelengths, the signal responses vary respectively as the 23rd, 14th, 13th, 10th, and 4th power of the absolute temperature.

The Earth's emissivity is highly variable from one surface to the next. Hence the ratio of signals at two of the GEM wavelengths is needed to obtain accurate surface-temperature measurements that depend very little on emissivity effects. For two bands at wavelengths λ_i and λ_j, the temperature response of the signal ratio R_{ij} is:

$$R_{ij} \cong (\epsilon_i/\epsilon_j)\, T^{[C_2/\lambda_i T_o - C_2/\lambda_j T_o]}. \quad (17)$$

Variations in the emissivity ratio are smaller by a factor of ten (or more) than variations in the absolute emissivity for different natural terrains. At the GEM wavelengths, where the radiation has the same spectral slope as a blackbody source, the emissivity ratio variations are very small. Thus, quantitative temperature measurements can be made, using signal ratios that are calibrated against a standard blackbody source. Data redundancy, obtained by detecting from three to five coregistered radiation signals, is expected to provide the most accurate surface-temperature measurements for varied natural terrains.

REFERENCES CITED

Anderson, D. N., and Axtell, L. H., eds., 1972, Geothermal overviews of the western United States: Geothermal Resources Council Compendium, El Centro Conference.

Dawson, G. B., and Dickinson, D. J., 1970, Heat flow studies in thermal areas of the north island of New Zealand: UN Symposium on the Development and Utilization of Geothermal Resources, Pisa, Proceedings (Geothermics Spec. Iss. 2) v. 2, pt. 1, p. 466.

Dickinson, D. J., 1973, Aerial infrared survey of Kawerau, Rotorua and Taupo urban areas: New Zealand Dept. Sci. and Indus. Research Geophys. Div. Rept. No. 89.

Godwin, L. H., Haigler, L. B., Rioux, R. L., White, D. E., Muffler, L. J. P., and Wayland, R. G., 1971, Classification of public lands valuable for geothermal steam and associated geothermal resources: U.S. Geol. Survey Circ. 647.

Hochstein, M. P., and Dickinson, D. J., 1970, Infrared remote sensing of thermal ground in the Taupo region, New Zealand: UN Symposium on the Development and Utilization of Geothermal Resources, Pisa, Proceedings, (Geothermics Spec. Iss. 2) v. 2, pt. 1, p. 420.

Hodder, D. T., Martin, R. C., Calamai, A., and Cataldi, R., 1973, Remote sensing of Italian geothermal steam field by infrared scanning: 1st Pan American Symposium on Remote Sensing, Panama City, Proceedings.

Larsen, L. M., 1971, Detector utilization in line scanners: Univ. of Michigan, Willow Run Labs. Rept., Infrared and Optics Dept., NASA Contract No. NAS9-9784.

LeSchack, L. A., and Del Grande, N. Kerr, 1975, Using airborne IR data as a geophysical tool is more than just photo-interpretation, abstract: Joint Convention of the Americal Society of Photogrammetry and the American Congress on Surveying and Mapping, Washington, D.C.

LeSchack, L. A., Del Grande, N. Kerr, Outcalt, S. I., Lewis, J., and Jenner, C., 1975, Correlation of dual-channel airborne IR data with soil moisture measurements: Silver Spring, Maryland, Development and Resources Transportation Company Final Rept., NOAA/NESS Contract No. 4-35308.

Loehwing, D. A., 1974, Hot competition—petroleum companies, utilities vie for energy from steam: Barron's Natl. Bus. and Finan. Weekly, v. LIV, no. 45, p. 3.

Lyon, R. J. P., 1964, Evaluation of infrared spectrophotometry for compositional analysis of lunar and planetary soils: rough and powdered surfaces: Stanford, California, Stanford Univ. Final Rept., Part 2, NASA Rept. No. CR-100.

*For small temperature excursions from T_o, where $T^{-1} = T_o^{-1}\left(1 + \frac{\Delta T}{T_o}\right)^{-1}$, $C_2/\lambda T$ is approximated by the first term of a binomial expansion (that is, $C_2/\lambda T_o$), which is a constant.)

Outcalt, S. I., 1972a, The development and application of a simple digital surface-climate simulator: Jour. Appl. Meteorology, v. 11, no. 4, p. 629.

——, 1972b, A reconnaissance experiment in mapping and modeling the effect of land use on urban thermal regimes: Jour. Appl. Meteorology, v. 11, no. 8, p. 1369.

——, 1972c, A synthetic analysis of seasonal influences in the effects of land use on the urban thermal regime: Archiv Meteorologie, Geophysik, u. Bioklimatologie, Serie B, v. 20, p. 253.

Palmason, G., Friedman, J. D., Williams, R. S., Jonsson, J., and Saemundsson, K., 1970, Aerial infrared survey of Reykjanes and Torfajokull thermal areas, Iceland: UN Symposium on the Development and Utilization of Geothermal Resources, Pisa, Proceedings (Geothermics Spec. Iss. 2), v. 2, pt. 1, p. 399.

Peck, E. L., Bissell, V. C., and Farnsworth, R. K., 1972, International field year for the Great Lakes—airborne snow reconnaissance: Silver Spring Maryland, Natl. Oceanic and Atmospheric Admin., Office of Hydrology, Hydrological Research Laboratory Interim Rept. No. 1.

Ray, D. L., 1973, The nation's energy future: Rept. of the Atomic Energy Commission to the President of the United States.

Saunders, P. M., 1970, Corrections for airborne radiation thermometry: Jour. Geophys. Research, v. 75, no. 36, p. 7596.

Shaw, R. W., and Irbe, J. G., 1972, Environmental adjustments for the airborne radiation thermometer measuring water surface temperature: Water Resources Research, v. 8, no. 5, p. 1214.

Standard Mathematical Tables, 1962, Integral no. 354: Chemical Rubber Company, 12th ed., p. 309.

Tien, C. L., 1974, Atmospheric corrections for airborne measurements of water surface temperature: Appl. Optics, v. 13, no. 8, p. 1745.

Vincent, R. K., 1973, A thermal infrared ratio imaging method for mapping compositional variations among silicate rock types [doctoral thesis]: University of Michigan.

Weiss, M., 1971, Airborne measurements of earth surface temperature (ocean and land) in the 10–12 and 8–14 micrometer regions: Appl. Optics, v. 10, no. 6, 1280.

White, D. E., and Miller, L. D., 1969, Calibration of geothermal infrared anomalies of low intensity in terms of heat flow, Yellowstone National Park (abstract): Am. Geophys. Union Trans. v. 50, p. 348.

An Airborne Infrared Survey of the Tauhara Geothermal Field, New Zealand

DAVID J. DICKINSON

Geophysics Division, Department of Scientific and Industrial Research, c/o Ministry of Works and Development, Wairakei, Private Bag, Taupo, New Zealand.

ABSTRACT

An airborne infrared survey has been flown over urban, industrial, and undeveloped land in the Tauhara and some other geothermal fields in New Zealand, using an Aga Thermovision model 665 camera, operating in the 4.5 to 5.5 μm band. Maps have been prepared from the thermograms which divide the surface temperatures into three ranges: at ambient temperature, 1 to 3°C above ambient, and more than 3°C above ambient. The 3°C contour coincides with the boundary between regions of conductive and convective heat flow determined from surface measurements. Methods have been developed for determining the heat flow from the infrared and other data. Some previously unknown areas of warm ground have been discovered and some thermal anomalies of nongeothermal origin identified and their effects eliminated. To assist the planning of industrial and urban development, it is intended to conduct similar surveys at approximately three yearly intervals to monitor any changes of the hydrothermal activity.

INTRODUCTION

During 1969, experimental aerial infrared (ir) surveys were flown over areas of hydrothermal activity near Taupo, New Zealand (Hochstein and Dickinson, 1970). The success of these tests and the experience gained from them led to a decision to fly infrared surveys at regular periods over several hydrothermal areas in order to monitor changes of the discharge areas. The first survey was flown in 1972 over the areas shown in Figure 1, and it is intended to repeat the surveys where possible, every three years.

Large-scale maps (1:2500) have been prepared showing the preliminary results of the 1972 survey in detail, and a report by Dickinson (1973) describes many aspects of that survey. The purpose of this paper is to describe some of the techniques used and results gained and to illustrate them with reference to the Tauhara field which borders the town of Taupo.

The Tauhara field has been chosen as its surface activity is varied and comprises such discharge features as warm and steaming ground, hot pools and springs, warm streams, and seepages. Activity, especially warm and steaming ground, is found within urban and industrial areas, as well as in the open country whose surface cover varies from grass to scrub and pine.

Recent population increases at Taupo have resulted in further residential and industrial development onto hydrothermal ground. The presence of this ground has caused engineering problems associated with house and factory siting, road construction, land utilization, electric power reticulation, and the installation of other services. Results of this survey will aid future planning of further development on active ground. Local authorities have already used some survey results to relocate roads and the sites of new buildings, including a high school.

Chemical and physical evidence (Dawson and Dickinson, 1970; Mahon, W. A. J., 1975, personal commun.; and others) suggests that the reservoirs of the Wairakei and Tauhara hydrothermal systems are interconnected and that the current exploitation of the Wairakei field may be influencing the activity of the Tauhara field. Since 1966, several changes in the surface activity of the Tauhara field have been noted,

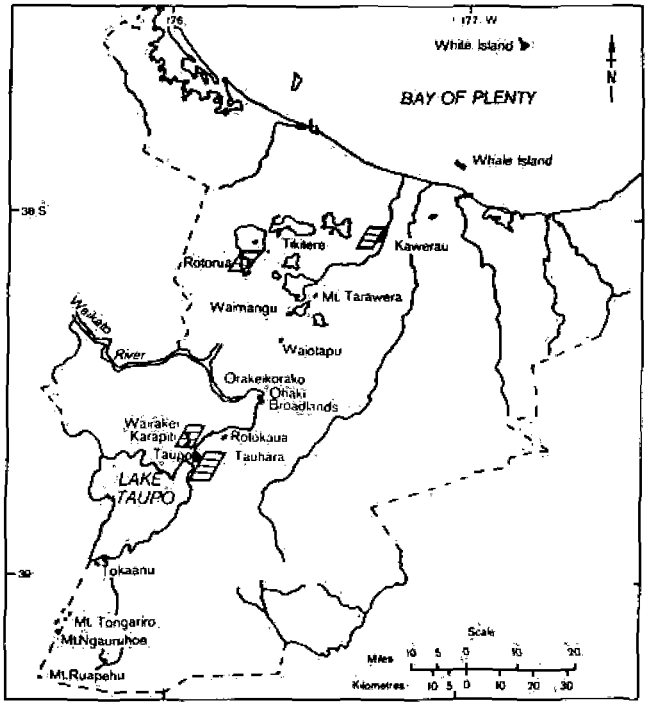

Figure 1. The volcanic zone, North Island, New Zealand. Hatched areas show the locations of the hydrothermal fields covered by the airborne infrared survey.

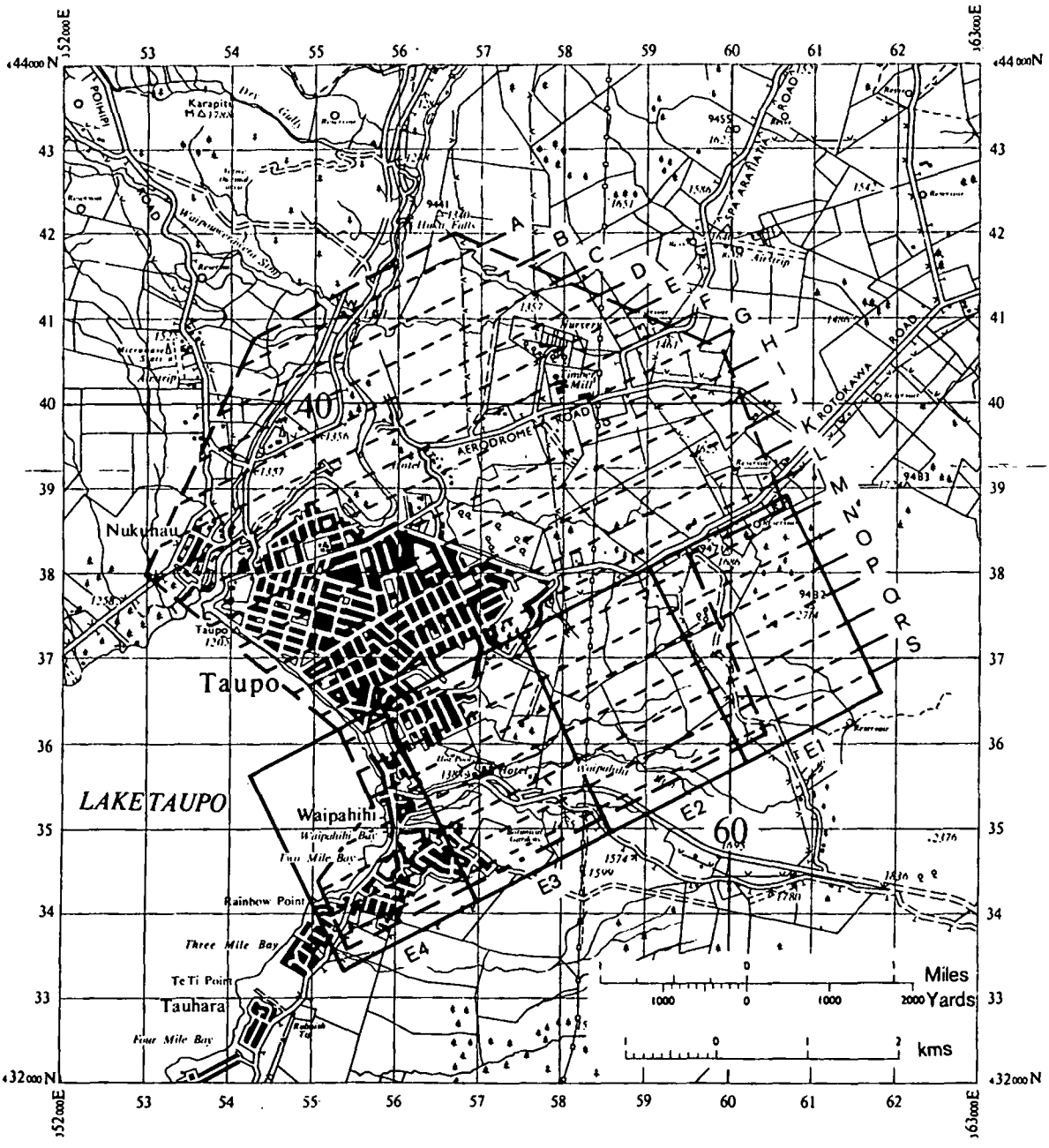

Figure 2. Flight lines and areas covered by the infrared survey of the Tauhara field. The areas E4, E3, and E2 are discussed in the text and shown in detail in Figures 3, 4, and 5.

including increases of some spring temperatures and increases of area and intensity of activity of some areas of warm and steaming ground. The infrared monitoring program should detect any further changes of thermal activity.

INSTRUMENTATION

The AGA Thermovision equipment (model 665) used for this survey was the same as that used for the 1969 studies and has been described by Borg (1968). The equipment, including camera and display unit, was fitted into a twin-engined Beechcraft AT-11 aircraft which had cameras and specialized equipment for aerial photography and mapping.

The infrared radiation being emitted from an object is detected by the AGA camera and converted into video signals which are pictured on a cathode ray tube at a rate of 16 frames per second. The thermal pictures (or imagery) which consist of 100 lines were recorded as photographs (or thermograms) by a Hasselblad model 500 EL camera. Relative temperature differences within the AGA camera's range of view appear as different shades of gray on the thermograms, the lighter shades representing areas with higher temperatures. As pointed out by Hochstein and Dickinson (1970), the spectral range normally detected by the AGA Thermovision is reduced from 2 to 5.6 μm to about 4 to 5.5 μm due to atmospheric absorption and other effects.

The Hasselblad camera was coupled to the aircraft's Zeiss RMK 60/23 aerial camera, which produced panchromatic photographs of the same area of ground as the thermograms. Both cameras were fired simultaneously at an average rate of one frame every 3.8 seconds.

METHOD

Full details of the field methods and interpretational techniques are given by Dickinson (1973). Because of aircraft availability and other reasons, the survey was flown in January and February (summer) 1972, although the atmospheric and radiation conditions of winter would have been more suitable. Flights were made during daylight hours because the Zeiss black-and-white photography was necessary to locate the thermograms and any anomalies appearing on them. Surveying was done during late afternoon and dusk. Fog and patches of low cloud prevented early morning surveying, while satisfactory results would have been unobtainable during the middle of the day because of the high levels of solar radiation.

The aircraft was flown at an altitude of about 1520 m above the ground, so that photography would be approximately at the scale of 1:2500 required for the final maps. Thermograms and the corresponding Zeiss photographs were overlapped by about 60% along each flight line, and by about 30% between adjacent flight lines. Flight lines and the area covered over the Tauhara field are shown in Figure 2.

At a test site on nonhydrothermal ground near Taupo, temperatures at the surface and at 0.05 m depth were monitored by a Taylor mercury-bulb thermograph. Infrared camera setting adjustments were made at the beginning of each flight period when flying over nonhydrothermal ground close to the test site. Adjustments were made so that the surface temperature of the ambient ground appeared as a dark-gray to near-black density on the cathode-ray screen. If necessary, final adjustments to this density, or background, were made when directly over the test site where thermograms were also taken. Further calibration runs were made at intervals during each flight period. Thermograms of the test site were used when required to calculate the ambient, or background, temperature for any flight run.

The gray tones on the thermograms were interpreted into three temperature ranges: less than 1°C above ambient temperature, between 1 and 3°C above ambient, and greater than 3°C above ambient. The regions in each of the temperature ranges were plotted onto halftone transparencies, or preliminary maps, having a scale of 1:2500 and representing a ground area of 4.6 km^2.

Areas of elevated temperature, obviously not of hydrothermal origin (roads, roofs, and so on) were deleted from the preliminary maps. Field checks of doubtful hydrothermal areas were made by temperature measurements at depths of 0.15 m and 1 m. Mostly, these were made to check isolated anomalies outside the main hydrothermal areas. A large number of temperature measurements were also taken to confirm surface boundaries of hydrothermal regions. In a few cases, isolated areas of 1 to 3°C anomalies suggested hydrothermal ground; but when checked, the anomalies proved to be of nonhydrothermal origin. They were usually caused by cover unusual to the area, such as moss and rock outcrops, and also by depletion of vegetation by stock. After checking temperatures on the ground, final halftone transparencies were prepared. Examples of the temperature anomalies from the final halftone

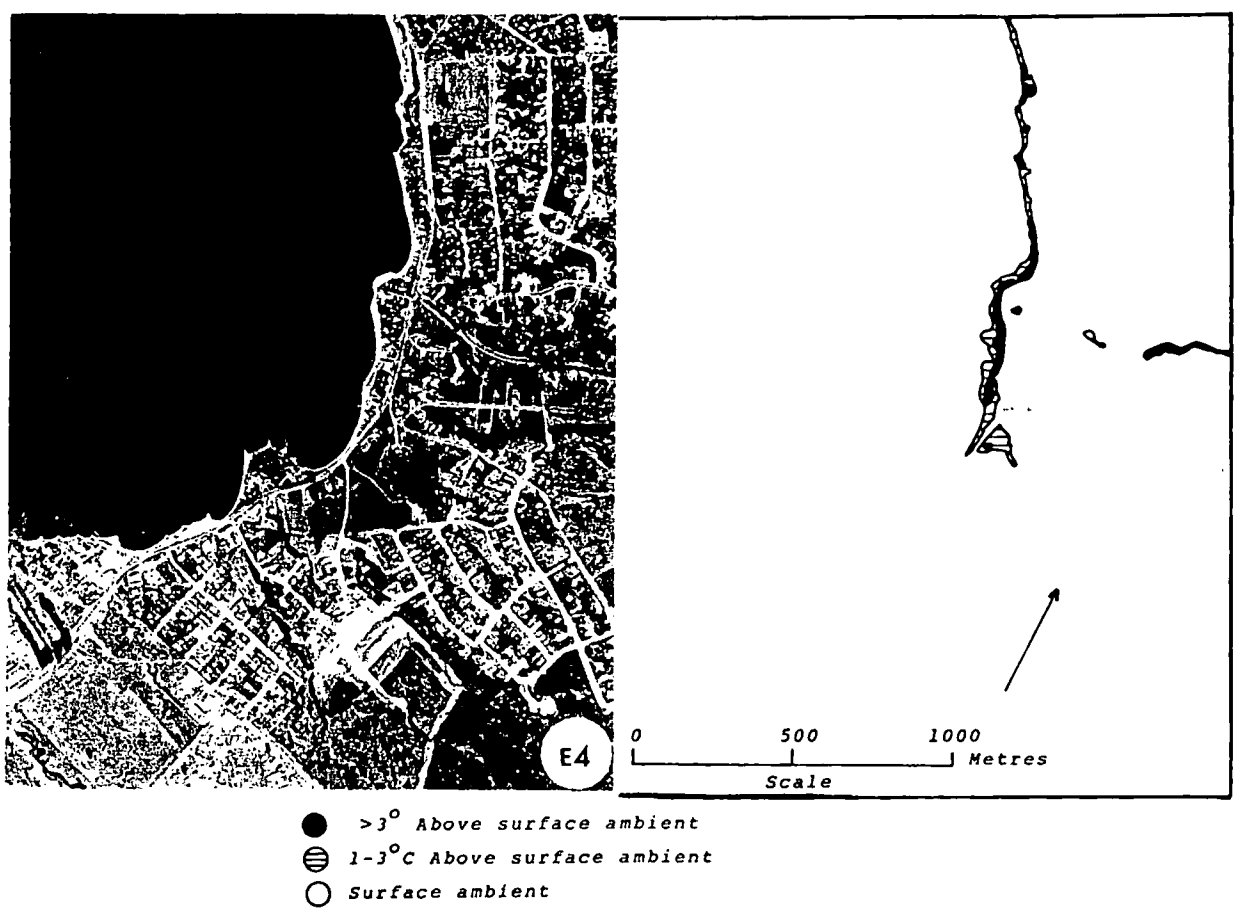

Figure 3. Black-and-white vertical aerial photograph and corresponding infrared surface temperature map for the area E4, shown in Figure 2.

maps of areas E4, E3, and E2 (in Fig. 2), and the corresponding panchromatic aerial photographs are shown in Figures 3, 4, and 5, respectively.

RESULTS AND DISCUSSION

Location and Monitoring of Hot Ground

As illustrated by the examples in Figures 3, 4, and 5, areas of hot ground have been outlined in great detail to an accuracy of a few meters. The locations of these areas agree with those mapped by Fisher (1964) but are in greater detail and are located more accurately. Some previously unknown hydrothermal features have been found, including a warm pool having an area of 6000 m^2.

It is planned to resurvey the Tauhara field in the winter of 1975. As well as indicating any changes that may have occurred in the hydrothermal activity, the resurvey will allow the relative merits of conducting infrared surveys in summer and winter to be assessed.

Interpretation of Thermograms

The interpretation of the three temperature regions appearing on thermograms was done visually. Figure 6 shows some examples of ir anomalies and their causes. Details of the anomalies and their interpretations are given in the caption of the figure. Feature 8 is ground at ambient temperature, features 1 and 6 are hydrothermal anomalies 1 to 3°C above ambient temperature, while features 5 and 7 are hydrothermal anomalies greater than 3°C above ambient. The other numbered features illustrate thermal anomalies of nonhydrothermal origin. Features 3 and 4 show that a bitumen road surface gives a thermal anomaly while a pumice road does not. Nonhydrothermal anomalies due to shingle and concrete surfaces are shown in features 2 and 9.

Thermograms covering areas of pine trees and scrub (manuka and broom) reveal some regions at ambient temperature and others in the range 1 to 3°C above ambient. Field checks of these 1 to 3°C areas, in most cases, confirmed these ground temperatures. Feature 1 in Figure 6 is an example of this. Robertson and Dawson (1964) show that in conductively heated ground the soil is dry near the surface. Murtha (1972) states that trees growing in soil deficient in moisture are warmer by 2 to 5°C than similar trees growing in normal conditions. Work by Myers et al. (1966) also shows that plants growing in dry soil have higher-than-normal leaf temperatures. Thus the temperature of the foliage of trees and scrub growing in conductively heated hydrothermal soil appears to be elevated by about the same amount as the ground surface beneath the canopy. Therefore, the presence of trees and scrub does not seriously disturb the infrared survey results.

Calculation of Heat Flow

Robertson and Dawson (1964) showed that in hydrothermal areas at places where the 1 m-depth temperature is less

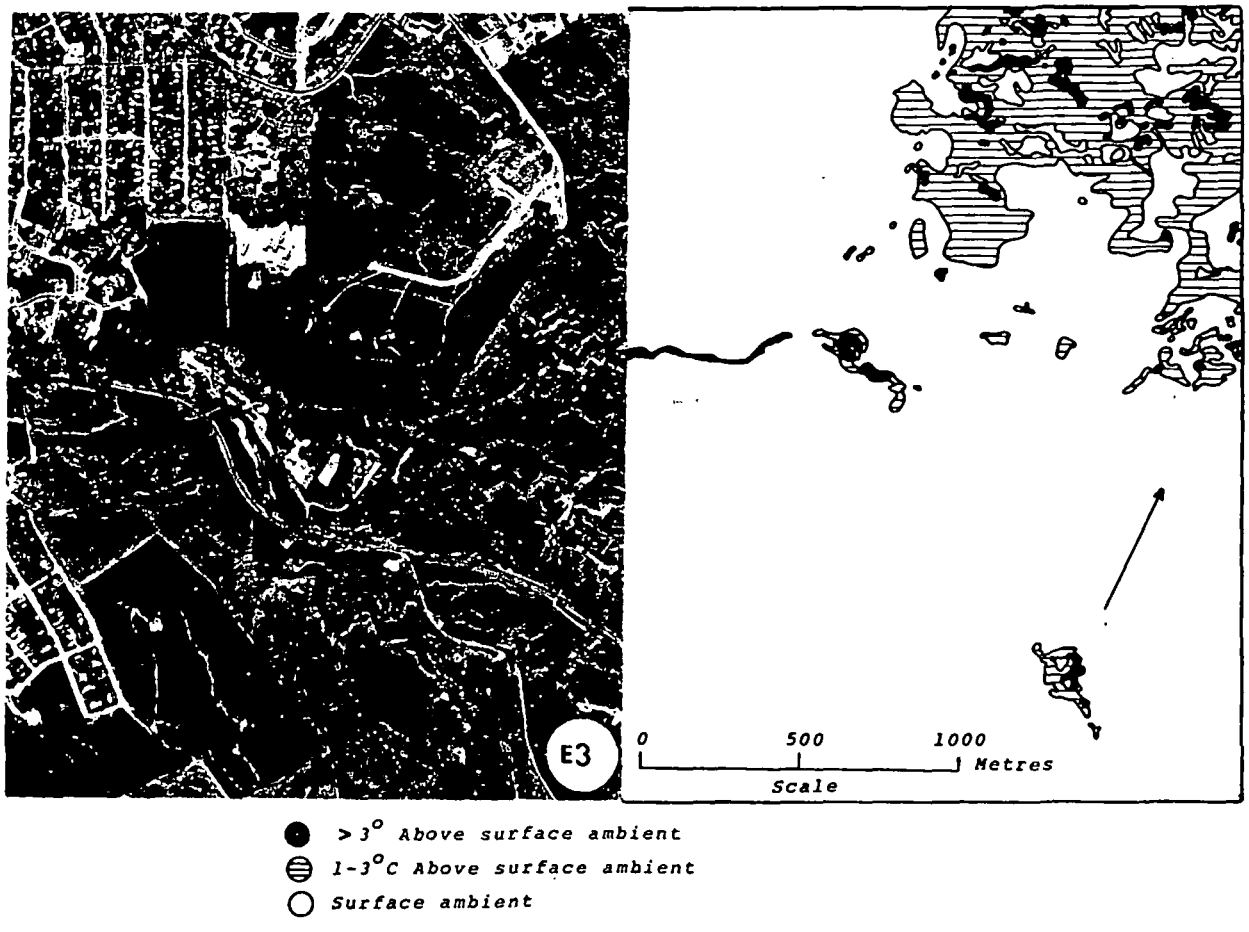

Figure 4. Black-and-white vertical aerial photograph and corresponding infrared surface temperature map for the area E3, shown in Figure 2.

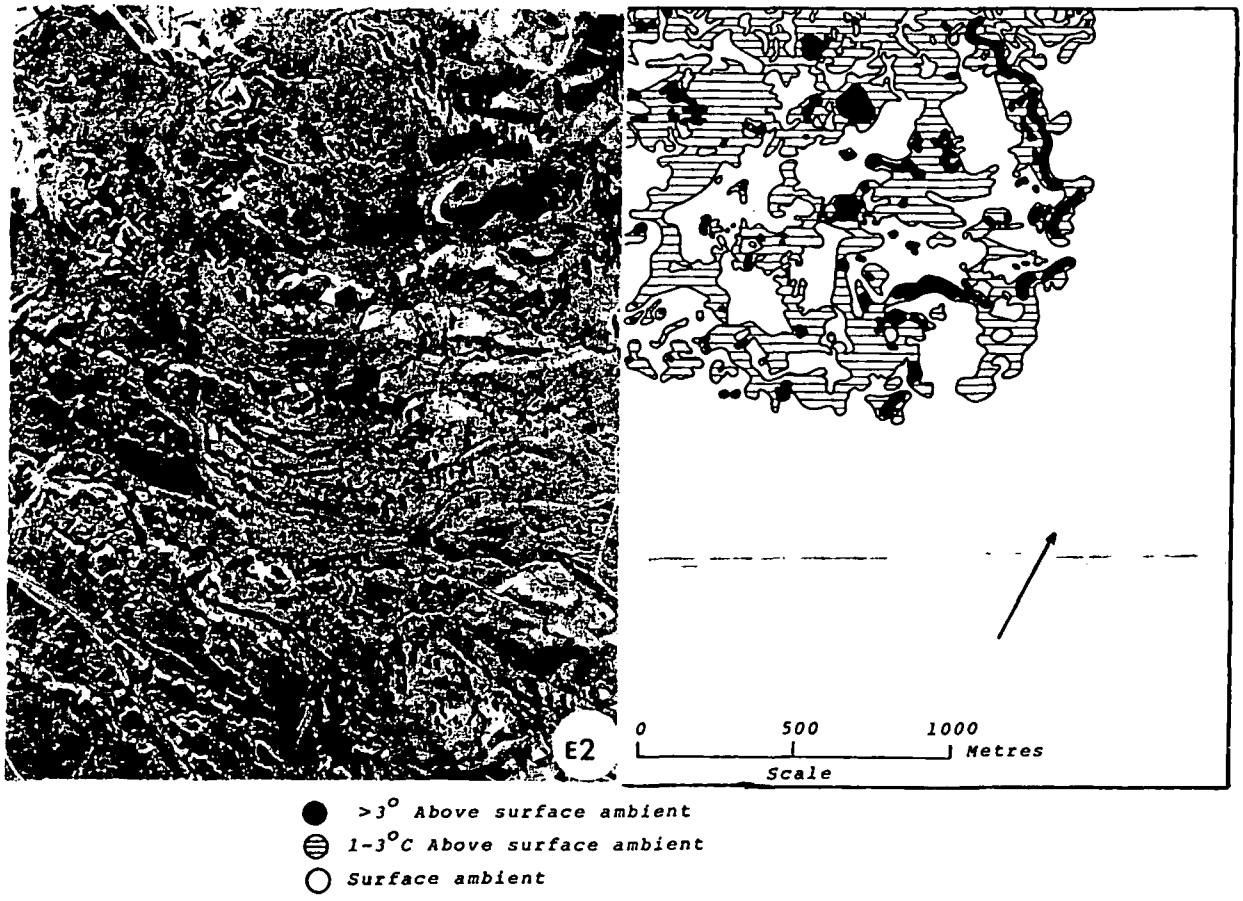

Figure 5. Black-and-white vertical aerial photograph and corresponding infrared surface temperature map for the area E2, shown in Figure 2.

than about 23°C above the ambient surface temperature, heat flow is predominantly conductive. Between 23 and 26°C above surface ambient, at 1 m depth, a transitional zone exists where heat flow is partly conductive and partly convective. Where the temperature at 1 m is in excess of 26°C above surface ambient, a convective heat flow predominates. It is shown in the papers by Dawson and Fisher (1964) and Dawson and Dickinson (1970) how extrapolations from 1 m temperatures can be made to obtain the temperature at 0.15 m depth. They also show how these temperatures, the type of surface vegetation, and of ground cover can be used to estimate the natural heat flow.

A series of temperature measurements at depths of 0.05, 0.15, 0.30 and 1.0 m were made when checking the ir hydrothermal anomalies. The measurements showed that the 3°C contour of the ir maps coincides approximately with ground temperatures of about 26°C above surface ambient at 1 m depth. Hence this contour represents the transitional region between conductive and convective heat flow. In the 1 to 3°C surface temperature regions, conductive heat flow predominates, and from Dawson and Fisher (1964), the heat flow value will be about 1 to 2 W/m^2. Where ir anomalies indicated surface temperatures above 3°C, 1 m-depth temperatures exceeded 26°C above ambient, showing that convection is the predominant heat flow mechanism. Heat flow values based on vegetation and surface cover from Dawson and Dickinson (1970) are given in Table 1.

Areas of various types of surface cover of the 3°C or greater surface temperature regions can be estimated from the survey's panchromatic photographs. By multiplying these areas by the corresponding heat flows expected for them, the heat flow for this type of ground can be obtained.

The heat loss from water surfaces was obtained differently. Areas of individual hot pools, streams, and seepages were measured from the thermograms and preliminary maps. Their temperatures were either measured in the field or calculated from the thermograms. From this information, the heat loss due to evaporation was obtained using the curves given by Dawson (1964).

An assessment of heat flow for part of the Tauhara field is shown in Table 2. A value of 110 MW was obtained for the natural heat flow from the areas E2, E3, and E4.

Table 1. Relationship between different types of ground cover distinguishable in black-and-white aerial photographs, infrared temperature anomalies, and heat flow.

Type	Ground cover	IR temperature anomaly (°C)	Heat flow (relative to 12°C) (W/m^2)
I	–	1–3	2
II	broom, leptosperms, small pines	>3	50
III	moss, lichens	>3	330
IV	thermal clays, algae, dead wood, bare ground, visible steam	>3	2 350
V	bare ground, steam vents	>3	12 600

Note: The ground cover and heat flow values, except for type I, were taken from Dawson and Dickinson (1970).

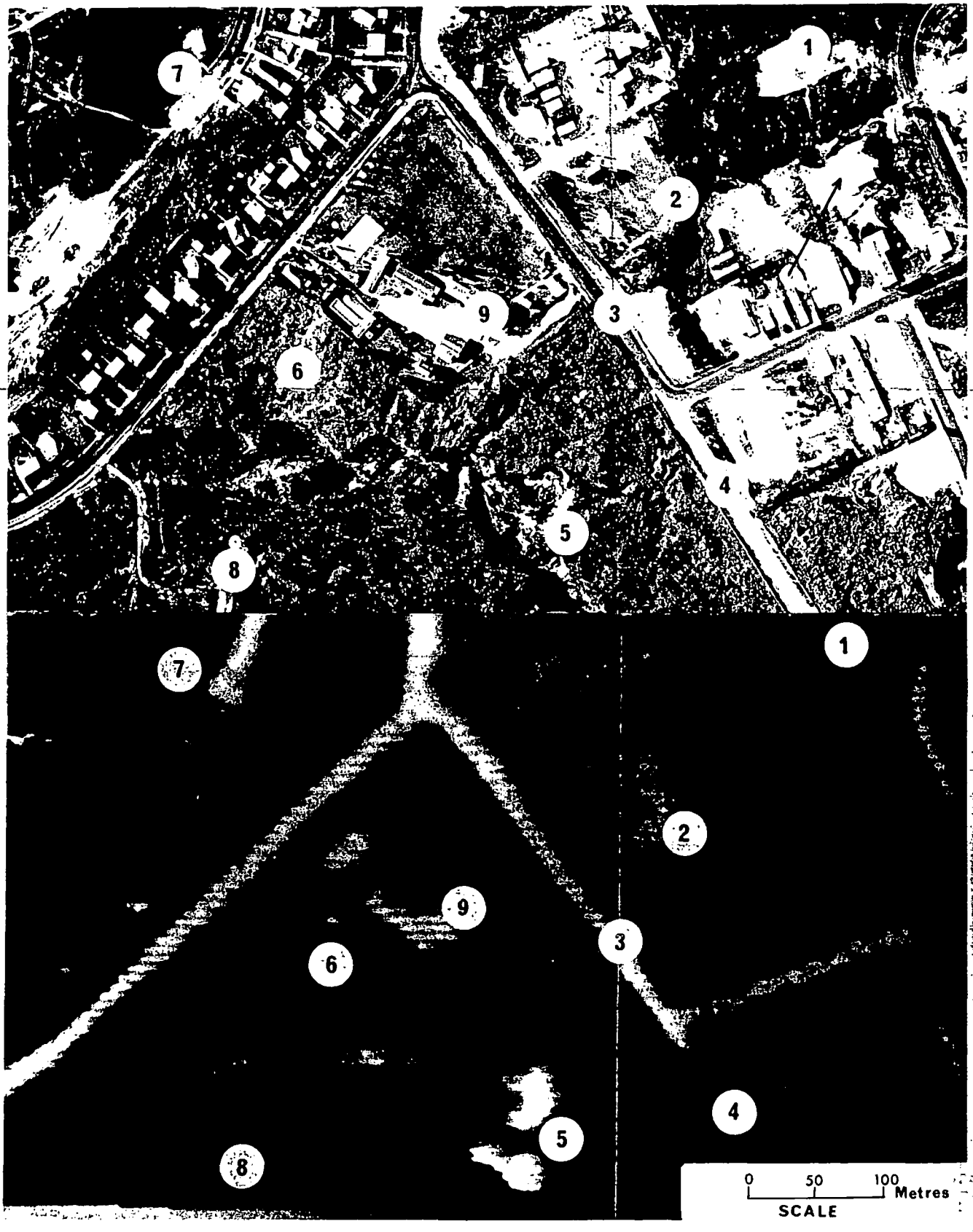

Figure 6. Black-and-white vertical aerial photograph and corresponding thermogram of an area of open country and developed land at grid reference 570/370 on Figure 2. Keys: (1) 1 to 3°C hydrothermal anomaly in scrub and pine; (2) nonhydrothermal anomaly on land covered with shingle; (3) nonhydrothermal anomaly on bitumen road surface; (4) pumice road showing only a small temperature anomaly; (5) >3°C hydrothermal anomaly in open country; (6) 1 to 3°C hydrothermal anomaly in open country; (7) >3°C hydrothermal anomaly in urban area; (8) area at ambient surface temperature; (9) >3°C nonhydrothermal anomaly over a concrete surface within a 1 to 3°C hydrothermal anomaly.

Table 2. Surface heat flow (relative to 12°C) from the parts of the Tauhara Field shown in Figures 3, 4, and 5.

Type (from Table 1)	Infrared anomaly °C	Figure 3 (E4) Area (m^2)	Figure 3 (E4) Heat flow (MW)	Figure 4 (E3) Area (m^2)	Figure 4 (E3) Heat flow (MW)	Figure 5 (E2) Area (m^2)	Figure 5 (E2) Heat flow (MW)	Totals Area (m^2)	Totals Heat flow (MW)
I	1–3	19 400	0.04	351 400	0.70	764 800	1.53	1 135 600	2.27
II	>3	17 200	0.89	23 100	1.16	84 600	4.23	124 900	6.28
III	>3			7 100	2.35	15 600	5.14	22 700	7.49
IV	>3			7 000	16.60	11 800	27.76	18 800	44.36
V	>3					1 625	20.48	1 625	20.48
Evaporation:									
pools and streams	1–3			1 250	1.04			1 250	1.04
	>3	5 700	6.70	8 875	14.00			14 575	20.70
seepage	1–3	11 500	8.20					11 500	8.20
Totals		53 800	15.83	398 725	35.85	878 425	59.14	1 330 950	110.82

Fisher (1965) estimated the heat flow of the entire Tauhara field to be 105 MW. This suggests that the ir method overestimates the natural flow. However, several factors should be considered. With the ir method, delineation of hydrothermal boundaries and areas is accurate, while the techniques available in 1964 relied a great deal on estimations. Since 1966 boundaries and intensities of warm and steaming ground have increased, as have temperatures of some hot springs and water surfaces (Dawson and Dickinson, 1970). The natural heat discharged from the nearby Karapiti area, part of the Wairakei system, has increased by some 400% between 1958 and 1968. Further intensity and area increases of warm and hot ground of the Tauhara area have also been noted after 1970. The 1964 assessment of heat loss from water surfaces and discharges may have also been underestimated. Fisher (1965) gives a seepage value of 3.78 MW for the E4 area (Fig. 3) and suggests that the figure of 6.30 MW given by Gregg (1958) was an overestimation. However, Gregg's value compares favorably with the 8.20 MW (Table 2) of this survey.

DAYLIGHT SURVEYS

Although other writers (cited by Murtha, 1972) claim that ir surveys utilizing the 3 to 5 μm wavelengths cannot be used during daylight hours to determine small temperature differences, because of dominant solar effects, satisfactory results were obtained in this survey. A possible explanation is that the lower heat capacity and thermal conductivity of the pumice soils in the Taupo area allow surface temperatures to attain near-equilibrium with the atmosphere by late afternoon. This would not be possible with many other soil types.

REFERENCES CITED

Borg, S. B., 1968, Thermal imaging with real time picture presentation: Appl. Optics, v. 7, p. 1697.

Dawson, G. B., 1964, The nature and assessment of heat flow from hydrothermal areas: New Zealand Jour. Geology and Geophysics, v. 7, p. 156.

Dawson, G. B., and Dickinson, D. J., 1970, Heat flow studies in thermal areas of the North Island of New Zealand: UN Symposium on the Development and Utilization of Geothermal Resources, Pisa, Proceedings (Geothermics, Spec. Iss. 2), v. 2 pt. 1, p. 466.

Dawson G. B., and Fisher, R. G., 1964, Diurnal and seasonal ground temperature variations at Wairakei: New Zealand Jour. Geology and Geophysics, v. 7, p. 114.

Dickinson, D. J., 1973, Aerial infrared survey of Kawerau, Rotorua and Taupo urban areas—1972; New Zealand Dept. Sci. and Indus. Research, Geophys. Div. Rept. No. 89, 53 p.

Fisher, R. G., 1965, Shallow heat survey of Taupo borough and adjacent country: New Zealand Jour. Geology and Geophysics, v. 8, p. 752.

Gregg, D. R., 1958, Natural heat flow from the thermal areas of Taupo sheet district (N94): New Zealand Jour. Geology and Geophysics, v. 1, p. 65.

Hochstein, M. P., and Dickinson, D. J., 1970, Infrared remote sensing of thermal ground in the Taupo region, New Zealand: UN Symposium on the Development and Utilization of Geothermal Resources, Pisa, Proceedings (Geothermics, Spec. Iss. 2), v. 2, pt. 1, p. 420.

Murtha, P. A., 1972, Thermal infrared line scan for forestry?: Ottawa, Ontario, Canadian Forest Serv. Dept. Environ., Forest Management Institute Information Report FMR-x-45, Study No. FM78, 46 p.

Myers, V. I., Wiegand, C. L., Heilman, M. D., and Thomas, J. R., 1966, Remote sensing in soil and water conservation research: 4th Symposium on Remote Sensing of Environment, Proceedings, p. 801.

Robertson, E. I., and Dawson, G. B., 1964, Geothermal heat flow through the soil at Wairakei: New Zealand Jour. Geology and Geophysics, v. 7, p. 134.